

The materialization of an impedimetric biosensor to detect papillomavirus DNA based on indium oxide nanowires

Peer-reviewed author version

SHOJAEI KOHNEHSHAHRI, Reza; Emame, Sourena Ramezani; Afrouz, Mohammad Mahdi & Shariati, Mohsen (2022) The materialization of an impedimetric biosensor to detect papillomavirus DNA based on indium oxide nanowires. In: APPLIED PHYSICS A-MATERIALS SCIENCE & PROCESSING, 128 (6) (Art N° 529).

DOI: 10.1007/s00339-022-05674-y

Handle: <http://hdl.handle.net/1942/37548>

# The materialization of an impedimetric biosensor to detect papillomavirus DNA based on indium oxide nanowires

S. H. Reza Shojaei <sup>a,b</sup>, Sorena Ramezani Emame <sup>b</sup>, Mohmmad mahdi Afrooz <sup>b</sup>, Mohsen Shariati <sup>\*a,c</sup>

<sup>a</sup> Department of Physics, Faculty of Science, Sahand University of Technology, P.O. Box, 5331817634, Tabriz, Iran

<sup>b</sup> X-LAB, Hasselt University, Agoralaan D, 3590, Diepenbeek, Belgium

<sup>c</sup> Manzaryeh Danesh School, Danesh Complex Institute, Tehran, Iran

\*Corresponding author's E-mail addresses: Shariatimohsen59@gmail.com

## ABSTRACT:

In this study, the impedimetric biosensor of human papillomavirus DNA (HPV DNA) in label free approach based on indium oxide nanowires ( $\text{In}_2\text{O}_3$  NWs) was fabricated. The fabrication of  $\text{In}_2\text{O}_3$  NWs was successfully conducted using thermal evaporation method and catalyst free approach. The grown NWs had a diameter of about 70 nm to 90 nm and length of several microns. The fabricated electrode was able to show high selectivity by changing the relative charge transfer resistance of 80, 60 and 50% for complementary, mismatch and non-complementary sequences, respectively. The electrode biosensor was stable for up to 6 weeks under the effect of electric field and showed 93% of its initial response sensitivity and detected DNA hybridization at very low concentrations in a linear response range from 0.1 pM to 0.1  $\mu\text{M}$ . The  $\text{In}_2\text{O}_3$  NWs showed a detection of limit (LOD) 20 fM. The behavior of negatively charged DNA oligonucleotides in a nanostructured array under the influence of electric field brought about NWs in the preferred direction with an excellent analytical response. Compared to current biosensors, the designed and fabricated biosensor, in a suitable sensing mechanism, was able to optimize response sensitivity and stability and also could improve the reproducibility conditions.

**Keywords: Biosensor; Papillomavirus;  $\text{In}_2\text{O}_3$  Nanowires; Impedance spectroscopy; Label-Free Mechanism.**

## 1. Introduction:

Human papilloma virus infection is a type of human papilloma virus (HPV), [1]. Most of the human papilloma virus infections are symptom-free and not resolved automatically, [1-4]. In some patients, the human papilloma virus infection causes warts or pre-cancerous ulcers, [1]. There are three classified categories, comprising about 200 types of papilloma viruses, depending on their role in the development of cervical cancer, they are denominated as low-risk, moderate and high-risk categories [2-8]. The high-risk genetic species of the HPV has a significant role in the engenderment of cervical cancer, and this is the third most common cancer in the post-endometrial women and ovarian cancer in the United States, [2]. The cancer resulted by HPV infection is one of the leading inducements of fatality worldwide and is the second leading cause of cancer depravity among women in developing countries, [2, and 8].

Among the 14 known high-risk species of the human papilloma viruses, two of them, subspecies HPV16 and HPV18 are the most important high-risk genotypes around the world and they have been monitored in 62% of cases related to cervical cancer. About 93% of the cervix related cancers can be prevented, thus their diagnosis and recognition are extremely vital, [2]. Due to its low sensitivity and specificity, the detection of the HPV via cell culture and serological testing may not be easily detected achievable, [2-4]. In contrast, molecular cervical cancer screening techniques including hybrid capture assay tests and polymerase chain reaction (PCR) are the efficient techniques for the detection of HPV, [4]. However, the mentioned techniques are basically dependent on the DNA sensing of viruses. However, the preparation and purification of samples in the mentioned techniques are very challenging and excessively time consuming [6-8].

Functional materials have been a strong candidate to overcome the problems originated from the lack of energy and systematic deficiencies [9-11]. The continuous evolution of nanoscience and nanotechnology in recent years has led to the production of quasi-one-dimensional structures in a variety of different morphologies such as NWs, core shell NWs, nanoribbons, nanotubes, **hierarchical heterogeneous micro and nanostructures, porous hollow nano-boxes nanosheets, layered paraelectric/ferroelectric nanocomposites polymers** [12-25], nanorods and nanopores [26-28]. Among the various nanostructured materials which have been produced, metal oxides have received special attention [29-30]. Metal oxide nanostructures have received a great deal of attention due to their fundamental properties and wide application in the manufacture of electronic **components** [31-34]. Among them,  $\text{In}_2\text{O}_3$ , with an optical gap of about 3.6 eV, has important applications in areas such as window heaters, solar cells, gas sensors, [26]. Recently,  $\text{In}_2\text{O}_3$  nanostructures have received considerable attention due to their new properties and applications in the field of bio-sensing [27], gas sensing [28, 35-38] and nano-transistors [39]. There has recently been a great deal of interest in the synthesis and research of  $\text{In}_2\text{O}_3$  nanostructures. Some of different  $\text{In}_2\text{O}_3$  nanostructures which have been obtained by different methods, such as CVD method [36 and 37], pulsed-laser [40], and oxide powder evaporation method [41], were applied to small analytes such as streptavidin [42].

Indium oxide recently has been used in biosensing and analyte measurements [37]. **In some reports, indium-based materials were used to HPV detection. Cervical cancer caused by HPV infection was investigated by A label free nano-sensing platform [43]. A fast, accurate and early detection platform was developed for HPV-16 detection in cost-effective label free DNA based on electrochemical biosensor. A low-cost and rapid electrochemical resistive DNA biosensor based on the current relaxation method was described [44]. A DNA probe, complementary to the specific human papillomavirus type 16 (HPV-16) sequence, was immobilized onto a screen-printed gold electrode. DNA hybridization was detected by applying a potential step of 30 mV to the system, composed of an external capacitor and the modified electrode DNA/gold, for 750  $\mu\text{s}$  and then relaxed back to the OCP, at which point the voltage and current discharging curves are registered for 25 ms.**

Electrochemical impedance spectroscopy (EIS) detection is one of the most promising mechanisms in label free bio-sensing especially in DNA detection. The EIS measurement studies the dielectric parameters of a biological system in wide frequencies, [45-48]. The EIS has demonstrated to provide information on wide basic processes such as surface adsorption, charge transfer, ion exchange and diffusion, [45-49]. The EIS provides the fundamental and functional information at the interface between the electrode and electrolyte, [45- 47]. The electrochemical impedance measurement system as a non-destructive and relatively facile to use detection system has been widely used in the field of label-free biosensors that are sensitive to cell culture monitoring, interaction between antibody and antigen [45-51], and DNA oligonucleotides hybridization, [46-49].

In this study, the impedimetric biosensor of HPV DNA based on  $\text{In}_2\text{O}_3$  NWs was fabricated. In this paper, the fabrication of  $\text{In}_2\text{O}_3$  NWs using thermal evaporation method in catalyst-free method in a horizontal tube furnace was successfully conducted. The fabricated electrode was able to give high

selectivity by changing the relative charge transfer resistance for complementary, mismatch and non-complementary sequences. The electrode biosensor was stable for several weeks under the effect of electric field and detected DNA hybridization at very low concentrations. The behavior of negatively charged DNA oligonucleotides in a nanostructured array under the influence of electric field brought about NWs in the preferred direction with an excellent analytical response. Compared to current biosensors, the designed and fabricated biosensor, in a suitable sensing mechanism, was able to optimize response sensitivity and stability and also could improve the reproducibility conditions.

## 2. Experimental section:

### 2.1. Materials

Potassium chloride,  $K_4Fe(CN)_6$ ,  $K_3Fe(CN)_6$ , ethanol, HCl, NaCl, EDTA (Ethylenediaminetetraacetic acid), and  $Na_3C_6H_5O_7$  were purchased from Merck. The PC template was obtained from Whatman Co. The Phosphate buffer saline (PBS), Dithiothreitol (D.T.T),  $NiSO_4 \cdot 6H_2O$ ,  $H_3BO_3$ ,  $KAu(CN)_2$ ,  $CH_2Cl_2$ , 3-aminopropyltriethoxysilane (APES), PVP (polyvinylpyrrolidone) were prepared from Sigma Aldrich.

### 2.2 Analyte preparation

The surface modification for HPV DNA probes immobilization on the Au-decorated nanowires (gold coated for FESEM imaging tendency) was performed in a sterilized clean room. Immobilization of thiolated oligonucleotides probe initially was performed after DNA preparation by DTT. PBS (6  $\mu$ L) (pH~4.5) containing 100  $\mu$ M single-stranded DNA probe was transported on the electrode, (modified nanowires) for 12 h. After DNA drop on the electrode surface, for removing some of the unabsorbed DNA oligonucleotides, the electrode system was submerged into 4mM 6- mercapto-1-hexanol for 1hr and then cleansed by PBS and DDW. For hybridization of SS-DNA probe with DNA target, first the probe electrode was submerged in PBS solution in pH~ 7.5, in concentration of 15  $\mu$ M SS-DNA target for 6 hr. It is important to note; target was part of the DNA sequence of the HPV and it was a complementary strand to the DNA probe. Finally, the sensing part of setup was cleansed with DDW and dried with argon gas in suitable flow. The buffers used in this work were as follows: DNA immobilization buffer: buffer Tris-EDTA (TE, 10 mM Tris-HCl, 1 mM EDTA, pH 8.0), hybridization buffer: 2 $\times$  saline sodium citrate (SSC, 300 mM NaCl, 20 mM  $Na_3C_6H_5O_7$ , pH 7.0). Electrolyte solution was 0.2 M KCl solution containing 2 mM  $K_4Fe(CN)_6/K_3Fe(CN)_6$  (1:1). All solutions were prepared in deionized water (DI water). 25-mer ss-DNA sequence with HS-( $CH_2$ )<sub>6</sub>-modification at the 5'-end with HPLC purification (as HPV 16 probe) and all target oligonucleotides with BIO-RP purification were provided. Stock solutions (100  $\mu$ M) of the DNA sequences were prepared with sterile distilled water (SD water) and stored at a refrigerator at -20 °C. Specificity of the oligonucleotide sequences were investigated with Basic Local Alignment Search Tool (BLAST) [5]. The used oligonucleotides sequences were listed in table 1.

**Table 1. The HPV16 DNA oligonucleotides sequences**

Sequence name	Sequence of oligonucleotides	Company (Country)
Thiolated-probe	5' - AAAGCAAAGTCATATACCTCACGTC - 3'	Bioneer Corporation (South Korea)
Complementary	5' - GACGTGAGGTATATGACTTTGCTTT - 3'	Bioneer Corporation (South Korea)
One-point Mismatch	5' - ACG CCA GAT GAA <u>GAA</u> GGG GAC GGT A - 3'	Bioneer Corporation (South Korea)
Non-complementary	5' - AACGTGAGGTATATGACTTTGCTTT - 3'	Bioneer Corporation (South Korea)

### 2.3 NWs fabrication

In this experiment, the used source was indium oxide powder. In this work, there was no catalyst. A number of P-type silicon substrates, which are immersed in ethanol alcohol solution for 20 minutes, were distilled twice in water solution for about 20 minutes. The amount of used powder was about 0.025 gr put in the alumina boat in the hot zone of the tube. The working process of the coating was followed; first the inside chamber was vacuumed by a rotary pump up to the allowable limit, a pressure of  $10^{-3}$  mbar. When the pressure reached to this level, the furnace temperature was raised to about 900 °C. Then argon gas was entered the chamber as a carrier gas in an alumina tube with a flow rate of 25 Scm. The duration of the deposition was about 2 hours. Finally, a white layer was settled on the substrates. The structural and crystalline properties of the samples were analyzed using XRD analyzer system by XRD device manufactured by Siemens Model 500D- ( $\lambda = 0.15419$  nm,  $\text{CuK}\alpha$ ) and surface properties were analyzed by FESEM analyzer by FESEM device (200FEG) made by Hitachi. A schematic illustration of this deposition process is shown in Fig. 1.

### 2.4. Electrochemical impedance spectroscopy measurements

Electrochemical impedance spectroscopy (EIS) measurements were conducted by a (PG STAT302N) automatic potentiostat equipped with a frequency response analyzer module (FRA32); (Autolab, Metrom, The Netherlands), associated with an electrochemical cell in a three-electrode system which Ag/AgCl was as reference, Pt as counter, and  $\text{In}_2\text{O}_3$  electrode as a working electrode. To plot Nyquist diagrams, Tecplot 360 software was used along with the computational fluid dynamic formats (CFD). EIS measurements were performed in the frequency range of 0.01-100 kHz and the disturbance potential was +10 mV. Measurements were performed under OCP conditions related to bias voltage. All EIS measurements were performed 3 times.

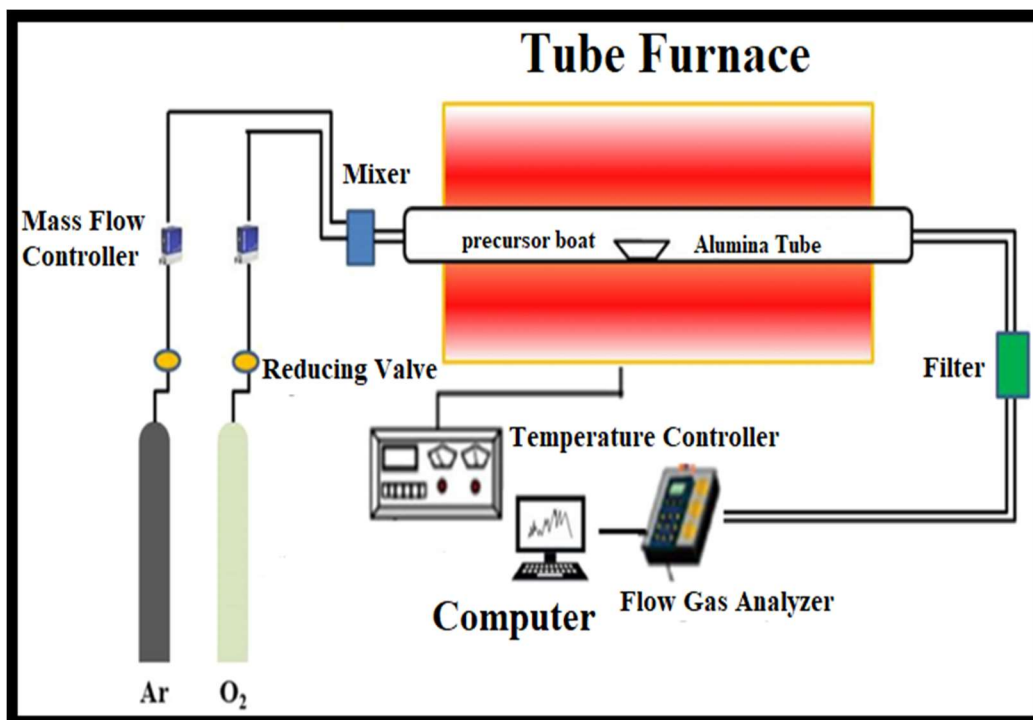


Fig. 1. Thermal evaporation furnace; Indium oxide deposition in the presence of argon gas,

### 3. Results and discussion

#### 3.1. Structural and surface analysis:

Fig. 2 shows the FESEM image of the fabricated samples. In this image, as can be seen, there are NWs with a diameter of 70 nm to 90 nm and a length of several microns. In such methods, the growth mechanism is usually called VS. In some methods associated with catalyst, it is clear that the catalytic nanoparticles are clearly visible at the end of the needle nanostructure. But there is no such thing in these NWs. The NWs have been grown in an uncontrollable direction due to the lack of catalysts. It can be seen that the needle like structures began to grow strongly from any point that causes to grow NWs in intertwined and intangible design. In this method, nucleation sites were created due to the use of VS mechanism by indium oxide vapor particles. This method does not require an external catalyst. The indium oxide atoms themselves provide these nucleation sites in a very interesting way and form these structures. The HRTEM and TEM measurements of an In<sub>2</sub>O<sub>3</sub> NW have been shown in Fig. 2D. In Fig. 2D the growth direction is coincided with the In<sub>2</sub>O<sub>3</sub> NWs. The crystallographic plane of In<sub>2</sub>O<sub>3</sub> for cubic crystal lattice by the inter-planar spacing of 0.512 nm related to the (200) crystallographic plane was validated in Fig. 2D. The growth direction of fabricated were oriented to [111], [28, 36-37].



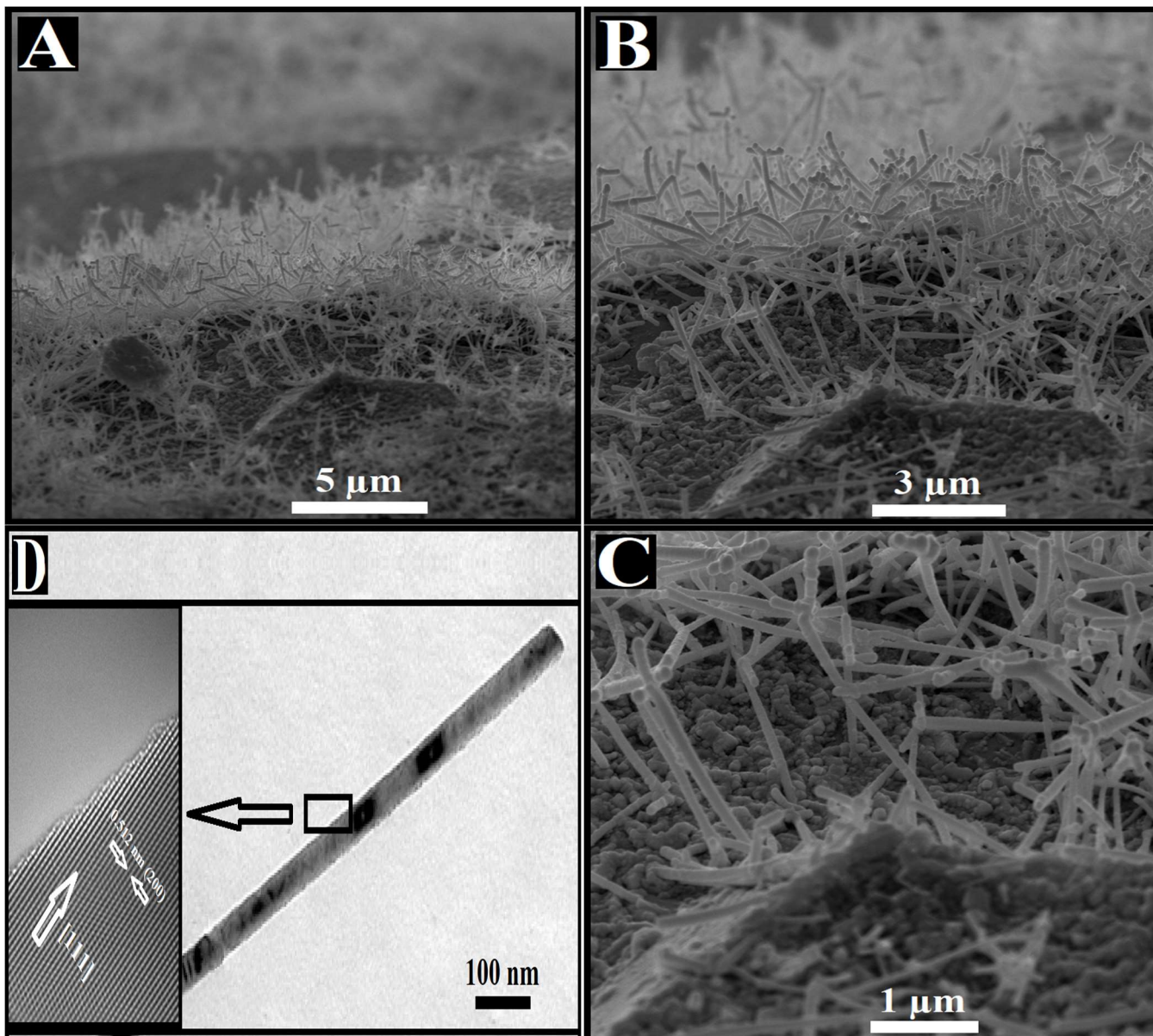


Fig. 2. The FESEM image of indium oxide NWs. The scale for A): 5  $\mu\text{m}$ , B): 3  $\mu\text{m}$  and C): 1  $\mu\text{m}$ , D) the HRTEM and TEM image of  $\text{In}_2\text{O}_3$  NW.

Fig. 3 shows the XRD analysis of the fabricated NWs. Interestingly, the formation of highly crystalline nanostructures occurs in one direction. It turns out that the formation of indium oxide structures is mainly significant in this regard. The absence of a catalyst can be attributed to the creation of related structures in an uncontrollable direction. The nanostructures created in this experiment are crystallized along a length that is completely arbitrary and random. According to the reference [36-37, 52], the cellular constant of these nanostructures is  $a = 1.012^\circ \text{ nm}$  according to JCPDS No. 6-0416.

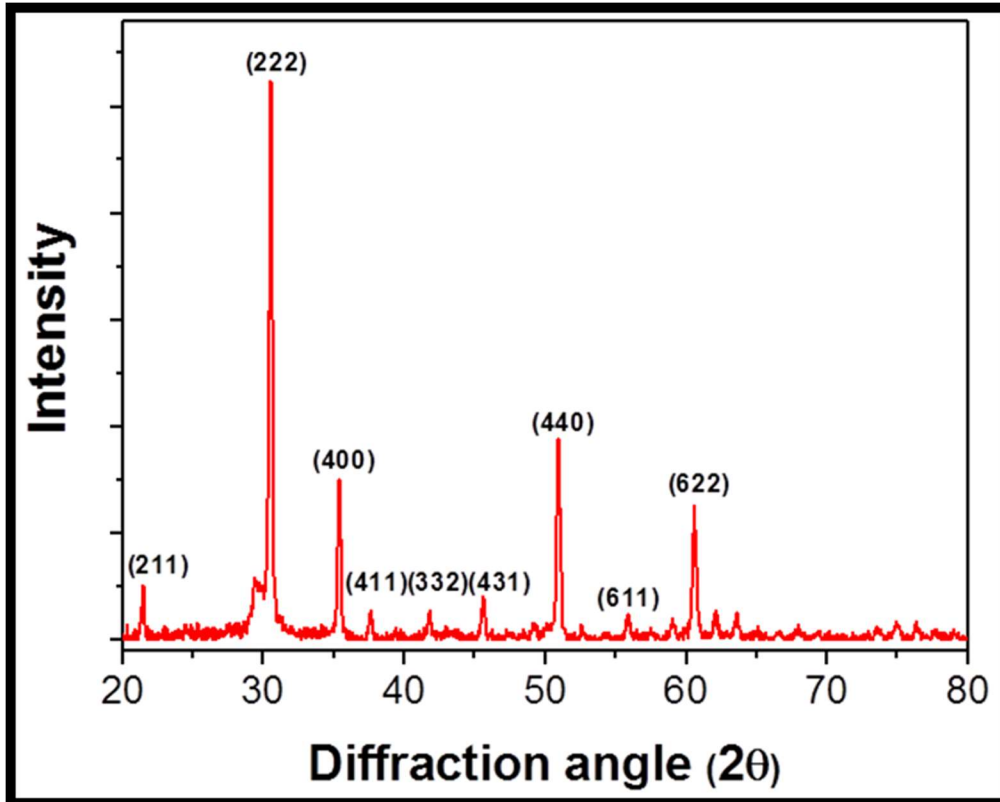


Fig. 3. Spectrum of indium oxide NWs by XRD analysis

### 3.2. Growth mechanism

There are two models to describe the growth mechanism of one-dimensional materials. The model associated with this section is a common torsional growth mechanism that emphasizes the existence of a rotational dislocation, which extends parallel to the axis of the wire or rod [26]. In this model, the plate rotates perpendicular to the dislocation line, causing the growth step to act as a low-energy site [26]. When the growth of NWs is achieved through direct condensation of the vapor phase without the use of a catalyst, the growth method used is called vapor-solid (VS) [26]. This method is sometimes called self-catalyst. In the past, this growth process was thought to be due to network defects, but when the NW was observed to be defective, this explanation was no longer acceptable. Another surprising effect recorded in this method is that the NW growth rate is higher than the computational density of the vapor phase. This can be interpreted as the plates in the NW structure absorbing the molecules that are later dispersed on the main growth surfaces of the wire. The VS process occurs in many non-catalytic growth processes. According to the information obtained from a series of relatively complete theoretical and experimental works, it has been shown that the minimization of surface free energy causes the growth of VS [26]. At high temperatures, the precursor material evaporates and then condenses directly on the substrate in the low temperature range. When the condensation process takes place, the molecules that are first condensed form catalytic granules, which act as nucleation sites [26]. As a result, they enable direct growth to minimize the surface energy that dominates the growth process. In other words, when indium oxide vapor particles are generated in the said conditions in a very hot region, they are transported by the carrier gas, which is argon gas, and land on the silicon substrate at a lower temperature [26]. These particles themselves cause the process of nucleation, adsorption and growth of NWs using the torsional growth process. In this type of growth, the NWs are bent and twisted, which is a good place to absorb molecules or clusters of vapor, which ultimately leads to one-dimensional growth of indium oxide NWs.



### 3.3. Sensory analysis

The sensing measurements were conducted in several tests such as; selectivity, response, stability, reproducibility, calculating the calibration curves and Randels equivalent circuit parameters. Fig. 4 shows the schematic image of DNA immobilization and hybridization on the NW surface. As shown in Fig. 4, the immobilization process could be materialized on the NW surface. For target hybridization which is coupling the single strand (probe) with complementary strand, the signal response would bring about the more charge carriers in the electrolyte. Uniform and continuous deposition of oligonucleotides on the NWs surface is a main parameter for DNA sensing. For non-complementary and mismatch sequences, the weak signal would be sensed. In weak hybridization, the response recording process would be conducted in low concentration of the charge carriers.

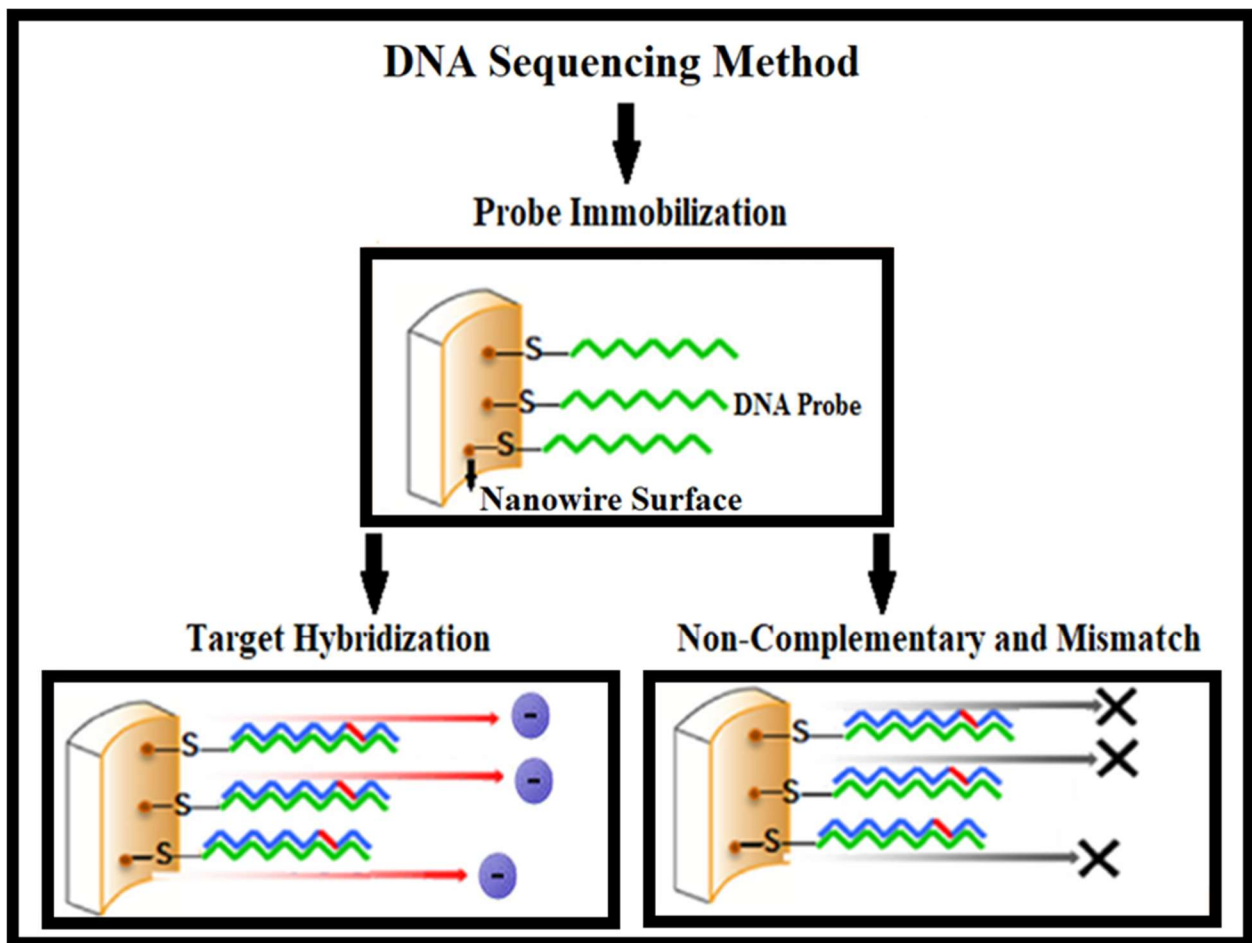


Fig. 4. the schematic image of DNA immobilization and hybridization on the NW surface

#### 3.3.1. Selectivity measurement for $\text{In}_2\text{O}_3$ electrode

Fig. 5 shows the EIS spectrum (Nyquist curve  $Z'$  vs.  $Z''$ ) using redox ions for the oligonucleotide-modified electrode. The Randles parameters;  $R_{ct}$ , CPE and  $R_s$  show the charge transfer resistance, the constant phase element at the interface between the electrode and the electrolyte, and the electrolyte resistance due to the uncompensated resistance to the solution associated with the internal resistance of the electrode and the resistance of the connections and wires, respectively. The  $Z_w$  (Warburg Impedance) resistance to the release of ferro/ferri ions in the electrode/electrolyte interfaces and in fact originates

from the redox couple diffusion and the electrode at low frequencies [53]. Results are obtained after three different independent tests for probe, complementary, mismatch and non-complementary DNA targets. All experiments were measured at a concentration of 1  $\mu\text{M}$ . Fig. 5 indicates the selectivity of the surface of an  $\text{In}_2\text{O}_3$  electrode with ss-DNA, complementary, non-complementary, and mismatch oligonucleotides. In Fig. 5, the EIS impedance spectra for the electrode modified with the ss-DNA probe and their hybridization for biosensors were investigated. As shown in Fig. 5, due to the compatibility and correlation of  $\text{In}_2\text{O}_3$  NWs with DNA targets, the diameter of the impedance semicircles of the  $\text{In}_2\text{O}_3$  electrode increased sharply in the presence of complementary oligonucleotides that show the reduction of the electrical conductivity of the  $\text{In}_2\text{O}_3$  electrode system. Fig. 5 shows that the  $\text{In}_2\text{O}_3$  modified electrode has significant DNA sensing capabilities. The corresponding charge transfer resistance ( $R_{ct}$ ) for dsDNA- $\text{In}_2\text{O}_3$  and ssDNA- $\text{In}_2\text{O}_3$  electrodes are 5618 and 1806 ohms, respectively. The diameter of the single-stranded DNA hybridization circle stabilized on the  $\text{In}_2\text{O}_3$  substrate with the complementary target strand increased compared to the non-complementary hybridization. The diameter of the probe hybridization semicircle compared to non-complementary hybridization increased with the target hybridization. This means that the charge transfer resistance enhanced with the formation of the complementary double layer and the change is around the value of  $\Delta R_{ct} = 3812 \Omega$ . Due to the electrostatic repulsion interactions, EIS measurements using non-complementary oligonucleotides indicate faster charge transfer kinetics and reduced resistance than the complementary single strand. However, in comparison to the immobilized complementary DNA strand, Nyquist plots show an enhancement in resistance when the non-complementary and single strand with a different base were used. Compared to probes, the electrostatic repulsion between the ferro/ferri redox couples and  $\text{In}_2\text{O}_3$  increases the charge transfer resistance. Also, the slope of the Warburg linear region for the complementary strand due to changes in the amount of penetration resistance of the charged species was reduced. By forming the double-stranded DNA, enhancement of the penetration resistance of charged species into the interface layer has increased the Warburg's impedance. Therefore, it causes that the mass transfer regime changes.

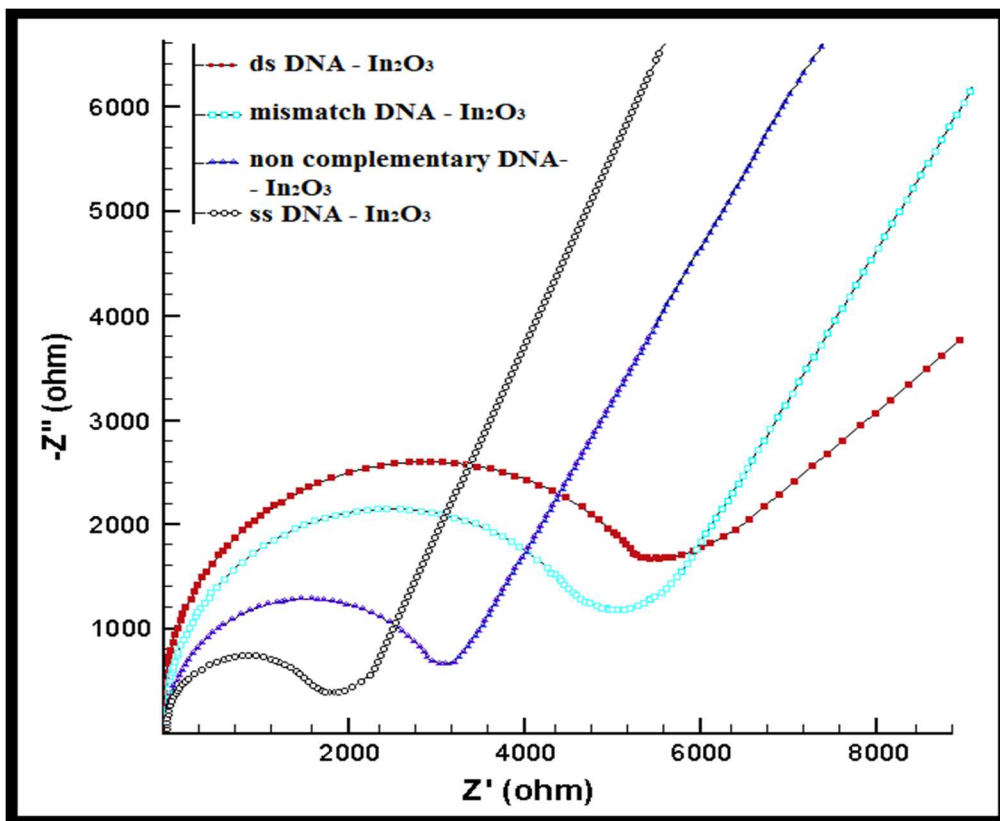


Fig. 5. The EIS impedance spectra for probes, complementary target, mismatch and non-complementary DNA oligonucleotides at 1  $\mu\text{M}$ . The electrolyte solution; 0.2 M KCl solution containing 2 mM  $\text{K}_4\text{Fe}(\text{CN})_6/\text{K}_3\text{Fe}(\text{CN})_6$  (1:1). Impedance spectra using AC modulation from +10 mV in the frequency range of 0.01 Hz to 100 kHz with DC bias without changes due to open circuit potential.

### 3.3.2. EIS response for $\text{In}_2\text{O}_3$ electrode

The sensitivity of the  $\text{In}_2\text{O}_3$  electrode response was examined in the presence of virus DNA. This study was performed by testing the response of the fabricated biosensor to different concentrations of complementary target oligonucleotides. The sensitivity of the biosensor response to complementary sequences for  $\text{In}_2\text{O}_3$  was measured from 0.1 pM to 0.1  $\mu\text{M}$  (Fig. 6). No satisfied response was recorded for concentrations less than 1  $\mu\text{M}$ . The  $\text{In}_2\text{O}_3$  electrode was able to respond to 0.1 pM. The amount of charge transfer resistance increased with increasing target DNA concentration of complementary. The strands of DNA molecules form a self-assembling single-layer on the electrode surface due to the strong covalent bond of thiol to gold [54]. Changes in charge transfer resistance have occurred due to conformational changes that occurred during DNA hybridization [54]. As the concentration of electroactive ions increases, the charge transfer resistance decreases. On the other hand, the enhancement of the concentration of complementary DNA led to an increase in charge transfer resistance due to the formation of compressed and aggregative layer. In fact, electrostatic interaction and spatial inhibition between ferro-ferri species and DNA phosphate group prevent ions from reaching the electrode surface and create a higher potential barrier for electron transfer of these species [54]. Also, the diffusion control zone has the lowest slope in the case of complementary filaments with higher concentration, which in turn is related to the more complete composition formed in the presence of complementary filaments at higher concentrations, which has the lowest possibility of mass transfer. However, it provides a self-aggregating monolayer on the surface of thiol-plated gold electrode [54].

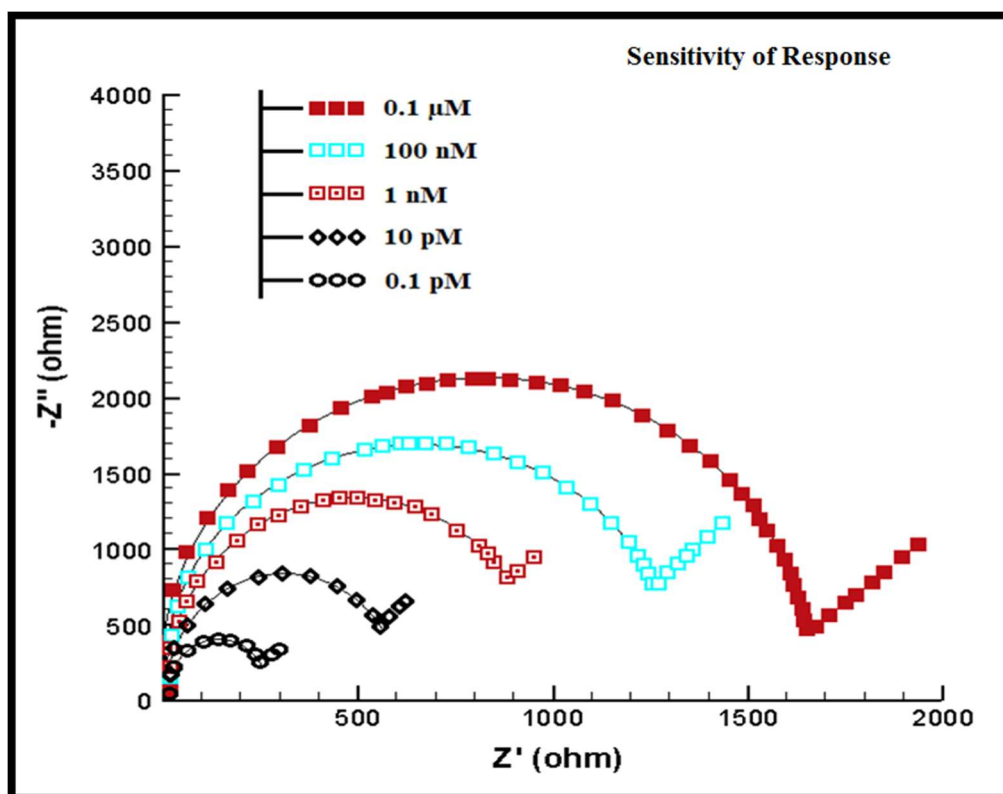


Fig. 6. EIS response measurements for  $\text{In}_2\text{O}_3$  electrode. Biosensor sensitivity to complementary sequences measured for  $\text{In}_2\text{O}_3$  from 0.1 pM to 0.1  $\mu\text{M}$ . the electrolyte solution 0.2 M KCl including 2 mM  $\text{K}_4\text{Fe}(\text{CN})_6/\text{K}_3\text{Fe}(\text{CN})_6$  (1: 1). Impedance spectra using AC modulation from + 10 mV in the frequency range of 0.01 Hz to 100 kHz with DC bias without changes due to open circuit potential

### 3.3.3. The stability test for fabricated $\text{In}_2\text{O}_3$ electrode

The stability of the  $\text{In}_2\text{O}_3$  electrode was investigated by storing biosensors in the freezer at 4°C after 6 weeks, and the results showed a maximum response for  $\text{In}_2\text{O}_3$  (at a concentration of 1  $\mu\text{M}$ ), and the  $\text{In}_2\text{O}_3$  biosensor was able to obtain 93% of its initial responses, (Fig. 7). This showed that the  $\text{In}_2\text{O}_3$  biosensor response has long-term stability.

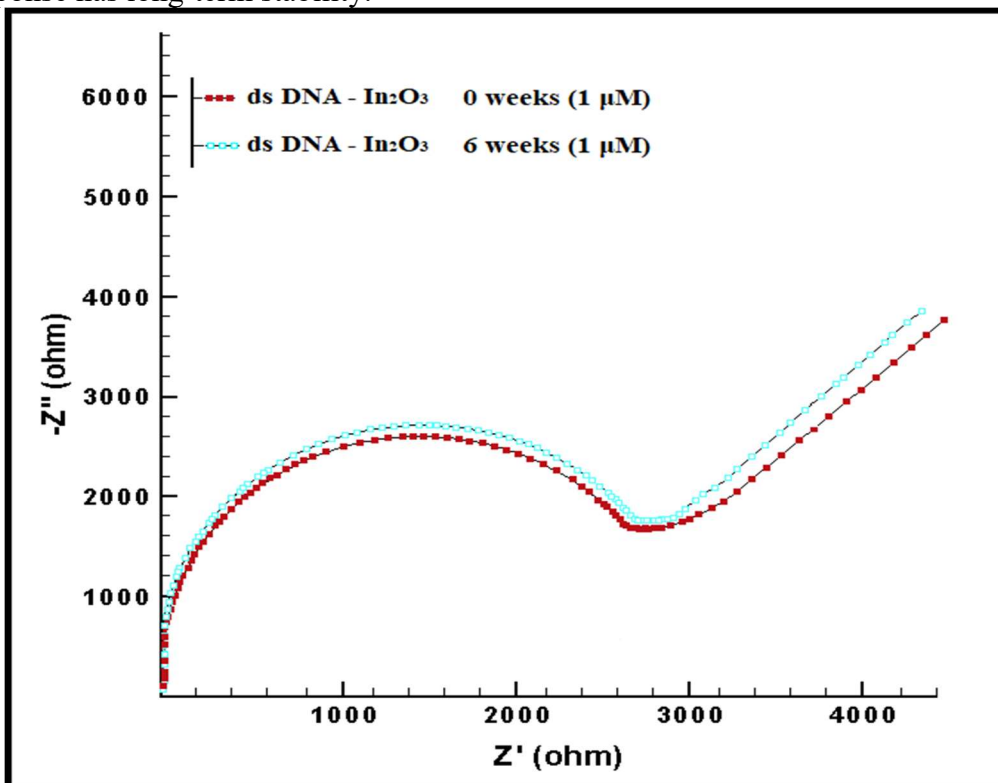


Fig. 7. Stability of  $\text{In}_2\text{O}_3$  electrode by storage in freezer at 4°C after 6 weeks (blue curve). Results of response to the complementary target (at a concentration of 1  $\mu\text{M}$ ). Recovery of 93% of the initial sensor response. Electrolyte solution; 0.2 M KCl solution containing 2 mM  $\text{K}_4\text{Fe}(\text{CN})_6/\text{K}_3\text{Fe}(\text{CN})_6$  (1: 1). Impedance spectra using AC modulation from + 10 mV in the frequency range of 0.01 Hz to 100 kHz with DC bias without changes due to open circuit potential.

### 3.3.4. Calibration curves for $\text{In}_2\text{O}_3$ electrode

Fig. 8 shows the calibration curve for the  $\text{In}_2\text{O}_3$  biosensor. Fig. 8 shows that changes in charge transfer resistance indicates a linear relationship with the logarithm scale of the concentration of complementary DNA sequences in the range of 0.1 pM to 0.1  $\mu\text{M}$  at the  $\text{In}_2\text{O}_3$  electrode (Fig. 8, blue line). The information diagram clearly shows a high sensitivity of the  $\text{In}_2\text{O}_3$  electrode response to the state without applying electrical potential. A detection limit of 20 fM was obtained for the  $\text{In}_2\text{O}_3$  electrode [2]. It was estimated  $Y = S_b + 3\sigma_b$  where  $S_b$  is the signal of blank and  $\sigma_b$  is the standard deviation of blank. The ability of the biosensor was tested by storing the biosensor in the freezer at 4°C for 6 weeks, Fig. 8 (red line). The results showed that the biosensor was able to maintain a maximum of 93% of its initial response after 6 weeks. This indicates that the impedimetric biosensor responses have been long-term stable.

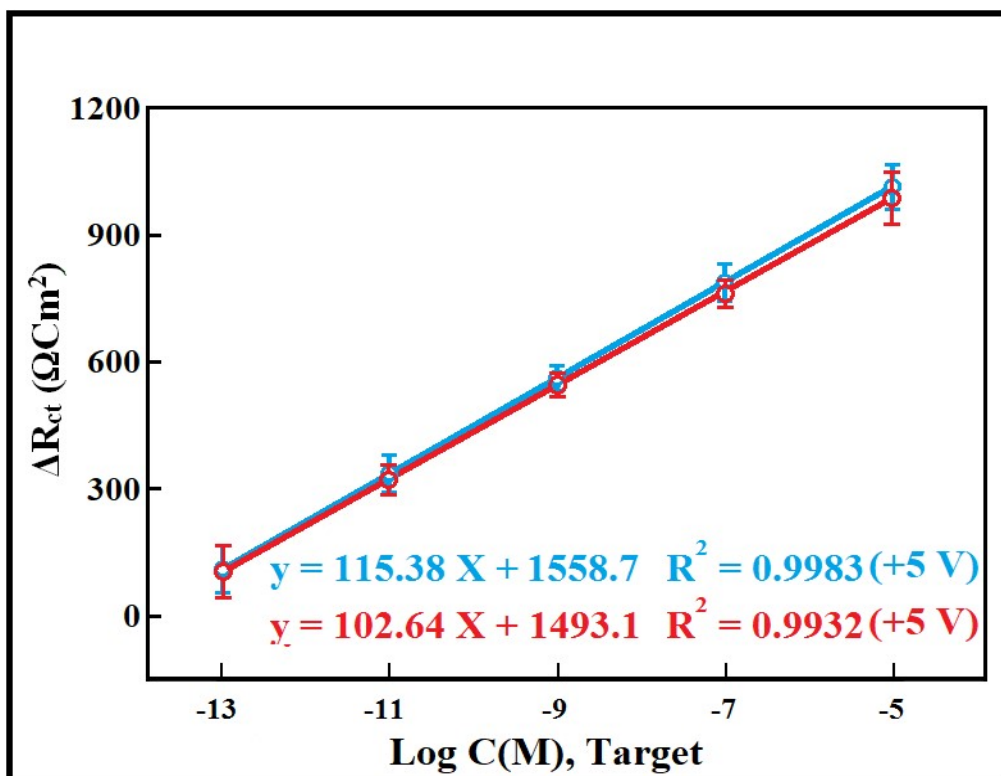


Fig. 8. Calibration curve for  $\text{In}_2\text{O}_3$  biosensor (blue line). Calculation of sensor stability after 6 weeks of maintenance (red line)

### 3.3.5. Reproducibility for $\text{In}_2\text{O}_3$ electrode

The reproducibility of the  $\text{In}_2\text{O}_3$  biosensor in DNA sensors was evaluated after calculating the data materialized by three independent electrodes fixed at a concentration of  $1 \mu\text{M}$ . Relative standard deviation (RSD) values for  $\text{In}_2\text{O}_3$  were 0.62, 3.26 and 5.96% for non-complementary, mismatch and complementary targets, respectively. RSD values of less than 9% indicated that the  $\text{In}_2\text{O}_3$  electrode had more acceptable biosensor detection than previous reports and have good accuracy for detecting and measuring HPV16 DNA [55, and 24 56].

### 3.3.6. Randels equivalent circuit parameters

The parameters of the Randels electric field elements obtained from the simulation of the impedance spectrum of the  $\text{In}_2\text{O}_3$  electrode are shown in Table 2. EIS measurements were consistent with the circuit elements. It can be said that the changes caused by the application of the field are quite noticeable. According to the conditions obtained, the higher sensitivity of the electrode can be achieved by fitting.

Table (2). Summary of Randels Equivalent Circuit Parameters for  $\text{In}_2\text{O}_3$  Electrode

Sample	$R_s(\Omega)$	CPE ( $10^{-6} \mu\text{F}$ )	N	$R_{ct}(\Omega)$	RSD (%)	$Z_w(10^{-5})$
SS-DNA	34	326	0.82	1806	1.37	8.93
dS-DNA	108	183	0.89	5618	2.16	3.11

### 3.3.7. The Comparison

In order to compare the quantification and qualification of the fabricated DNA biosensor, the performance of the several recently published works are summarized in Table 3. The results in Table 3 also showed that the electrochemical response of the In<sub>2</sub>O<sub>3</sub> electrode shows satisfied performance and has better response. The experimental results reported in this study evidently demonstrate the effects of In<sub>2</sub>O<sub>3</sub> electrode structure on the improvement of DNA sensor detection sensitivity.

**Table 3. the comparison of the quantification and qualification of the fabricated HPV DNA biosensors.**

<b>Biosensor</b>	<b>Electrode</b>	<b>Method</b>	<b>Concentration Range</b>	<b>LOD</b>	<b>REF.</b>
biosensor based on labeled pyrrolidinyI peptide	screen-printed carbon electrodes	SWV	0.02–12 $\mu$ M	4 nM	[57]
DNA biosensor for HPV 16	Gold electrode	DPV	18–250 nM	18 nM	[58]
Biosensor for short DNA Sequences	Screen-printed gold electrodes	SWV	0–770 pM	0.308 pM	[6]
papilloma virus DNA biosensor using SWCNT	Single walled carbon nanotube	EIS	1aM-1 $\mu$ M	1 aM (Atto molar)	[4]
DNA biosensor to identify a target gene cloned into a plasmid	Pencil graphite electrode	DPV	5.36-670 nM	2 nM	[59]
a pencil graphite (lead) electrode (PGE) for the detection of HPV	Pencil graphite electrode	SWV	185 –7700 nM	185 nM	[60]
An amperometric sensor for papillomavirus	Carbon nano-onion modified glassy carbon	Amperometry	0–20 nM	0.5 nM	[61]
Impedimetric biosensor to detect papillomavirus	In <sub>2</sub> O <sub>3</sub> NWs	EIS	0.1 pM to 0.1 $\mu$ M	20 fM	This work

#### 4. Conclusion:

A DNA biosensor was developed to detect human papillomavirus based on indium oxide NWs in asymptomatic mechanisms and electrochemical impedance measurements, as well as in accordance with the Randles equivalent circuit. The indium oxide NWs were successfully performed in a horizontal tube furnace using thermal evaporation method without the use of catalysts. The ss-DNA single-stranded DNA probe was covalently immobilized on the surface of the In<sub>2</sub>O<sub>3</sub> NWs electrode by the thiol agent. The In<sub>2</sub>O<sub>3</sub> electrode biosensor detected HPV DNA hybridization at very low concentrations in a linear response range from 0.1 pM to 0.1  $\mu$ M. In<sub>2</sub>O<sub>3</sub> electrode biosensor was able to achieve a diagnostic limit of 20 fM. In<sub>2</sub>O<sub>3</sub> electrode was able to make a strong differentiation between complementary, non-complementary and mismatch DNA sequences and was able to obtain high selectivity by changing the



relative charge transfer resistance of 80, 60 and 50% for complementary, mismatch and non-complementary sequences, respectively. The In<sub>2</sub>O<sub>3</sub> electrode biosensor was stable for up to 6 weeks and showed 93% of its initial detection response.

## 5. Funding and/or Conflicts of interests/Competing interests

The authors declare that they have no known competing financial interests or personal relationships that could have appeared to influence the work reported in this paper. There is no funding in this work.

### References:

- [1] M Van Ranst, JB Kaplan, RD Burk, Phylogenetic classification of human papillomaviruses: correlation with clinical manifestations. *J Gen Virol* (1992) 73(10):2653–2660
- [2] Laís Canniatti Brazaca, Pãmyla Layene Dos Santos, Paulo Roberto de Oliveira, Diego Pessoa Rocha, Jéssica Santos Stefano, Cristiane Kalinke, Rodrigo Alejandro Abarza Muñoz, Juliano Alves Bonacin, Bruno Campos Janegitz, Emanuel Carrilho, Biosensing strategies for the electrochemical detection of viruses and viral diseases—A review, *Analytica Chimica Acta*, (2021) 1159, 338384
- [3] M Shariati, M Ghorbani, P Sasanpour, A Karimizefreh, An ultrasensitive label free human papilloma virus DNA biosensor using gold nanotubes based on nanoporous polycarbonate in electrical alignment, *Analytica chimica acta* (2019)1048, 31-41;
- [4] S Wang, L Li, H Jin, T Yang, W Bao, S Huang, J Wang, Electrochemical detection of hepatitis B and papilloma virus DNAs using SWCNT array coated with Au nanotubes. *Biosens Bioelectron* (2013) 41:205–210.
- [5] M Shariati, Impedimetric Biosensor for Monitoring Complementary DNA from Hepatitis B Virus Based on Gold Nanocrystals, *J. Electrochem. Soc.* (2021) 168; 016512
- [6] N Zari, A Amine, MM Ennaji, Label-free DNA biosensor for electrochemical detection of short DNA sequences related to human papilloma virus. *Anal Lett* (2009) 42(3):519–535.
- [7] N Nasirizadeh, HR Zare, MH Pournaghi-Azar, MS Hejazi, Introduction of hematoxylin as an electroactive label for DNA biosensors and its employment in detection of target DNA sequence and single-base mismatch in human papilloma virus corresponding to oligonucleotide. *Biosens Bioelectron* (2011) 26(5):2638–2644.
- [8] LD Tran, DT Nguyen, BH Nguyen, QP Do, H Le Nguyen, Development of interdigitated arrays coated with functional polyaniline/MWCNT for electrochemical biodetection: application for human papilloma virus. *Talanta* (2011) 85(3):1560–1565.

- [9] Q. Chu, Z. Sun, Y. Liu, H. Cui, B. Cheng, D. Dastan, K. Moon, G. Yang, C. Wong, Difluorobenzylamine Treatment of Organolead Halide Perovskite Boosts the High Efficiency and Stability of Photovoltaic Cells *ACS Appl. Mater. Interfaces* (2022), 14, 9, 11388–11397
- [10] S. Xia, Z. Shi, L. Sun, S. Sun, D. Dastan, R. Fan, Suppressing the loss and enhancing the breakdown strengths of high-k materials via constructing layered structure, *Mater. Lett.* (2022) 312; 131654.
- [11] M Shariati, A Mallakin, F Malekmohammady, F Khosravi-Nejad, Inhibitory effects of functionalized indium doped ZnO nanoparticles on algal growth for preservation of adobe mud and earthen-made artworks under humid conditions, *International Biodeterioration & Biodegradation* (2018) 127, 209-216;
- [12] L. Liang, Z. Shi, X. Tan, S. Sun, M. Chen, D. Dastan, B. Dong, L. Cao, Largely Improved Breakdown Strength and Discharge Efficiency of Layer-Structured Nanocomposites by Filling with a Small Loading Fraction of 2D Zirconium Phosphate Nanosheets, *Adv. Mater. Interfaces* (2021), 2101646.
- [13] M. Kartha, B. Reshi, P. Walke, D. Dastan, Morphological Study of Thin Films: Simulation and Experimental Insights using Horizontal Visibility Graph, *Ceram. Int.* 48 (2022) 5066-5074.
- [14] L. Tao, J. Huang, D. Dastan, J. Li, X. Yin, Q. Wang, Flue Gas Separation at Organic-Inorganic Interface under Geological Conditions, *Surf. Interfaces* (2021) 27 ;101462.
- [15] M Shariati, F Khosravinejad, The laser-assisted field effect transistor gas sensor based on morphological zinc-excited tin-doped  $\text{In}_2\text{O}_3$  nanowires, *Surface Review and Letters*, (2017) 24 (08), 1750113;
- [16] M Shariati, The continuous and persistent periodical growth induced by substrate accommodation in  $\text{In}_2\text{O}_3$  nanostructure chains and their photoluminescence properties. *Applied Physics A* (2015)118 (3), 997-1007,
- [17] M. Han, Z. Shi, W. Zhang, K. Zhang, H. Wang, D. Dastan, R. Fan Significantly Enhanced High Permittivity and Negative Permittivity in  $\text{Ag}/\text{Al}_2\text{O}_3/3\text{D-BaTiO}_3/\text{epoxy}$  Metacomposites with Unique Hierarchical Heterogeneous Microstructures, *Compos: Part A*, (2021) 149 106559.
- [18] M Shariati, M Darjani, The lateral  $\text{In}_2\text{O}_3$  nanowires and pyramid networks manipulation by controlled substrate surface energy in annealing evolution. *Journal of Crystal Growth* (2016) 436, 104-112,
- [19] M. Zhang, Z. Shi, J. Zhang, K. Zhang, L. Lei, D. Dastan, B. Dong, Greatly Enhanced Dielectric Charge Storage Capabilities of Layered Polymer Composites Incorporated with low loading fractions of Ultrathin Amorphous Iron Phosphate Nanosheets, *J. Mater. Chem. C*, (2021), 9, 10414.
- [20] M Shariati, The Cancer therapy materialization by Theranostic nanoparticles based on gold doped Iron oxide under electromagnetic field amplification, *Nanomedicine: Nanotechnology, Biology and Medicine*; (2021) 35, 102406
- [21] L. Sun, Z. Shi, B. He, H. Wang, S. Liu, M. Huang, J. Shi, D. Dastan, H. Wang, Asymmetric Trilayer All-Polymer Dielectric Composites with Simultaneous High Efficiency and High Energy Density: A Novel Design Targeting for Advanced Energy Storage Capacitors, *Adv. Funct. Mater.* (2021), 2100280.

- [22] S. Wei, Z. Shi, W. Wei, H. Wang, D. Dastan, M. Huang, J. Shi, S. Chen, Facile preparation of ultralight porous carbon hollow nanoboxes for electromagnetic wave absorption, *Ceram. Int.*, (2021) 47; 28014–28020.
- [23] S. Sun, Z. Shi, L. Sun, L. Liang, D. Dastan, B. He, H. Wang, M. Huang, R. Fan, Achieving Concurrent High Energy Density and Efficiency in All Polymer Layered Paraelectric /Ferroelectric Composites via Introducing a Moderate Layer, *ACS Appl. Mater. Interfaces*, (2021), 13, 27522–27532.
- [24] Y. Jiao, Z. Huang, W. Hu, X. Li, Q. Yu, Y. Wang, Y. Zhou, D. Dastan, In-situ hybrid Cr<sub>3</sub>C<sub>2</sub> and  $\gamma$ -Ni<sub>3</sub>(Al, Cr) strengthened Ni matrix composites: microstructure and enhanced properties, *Mater. Sci. Eng. A*, (2021) 820 ;141524.
- [25] N. Haghnegahdar, M. Abbasi Tarighat, D. Dastan, Curcumin-functionalized nanocomposite AgNPs/SDS/ MWCNTs for electrocatalytic simultaneous determination of dopamine, uric acid, and guanine in co-existence of ascorbic acid by glassy carbon electrode, *J Mater Sci: Mater Electron* (2021) 32:5602–5613.
- [26] J. G. Lu, P. Chang and Z. Fan; "Quasi-one-dimensional metal oxide materials.Synthesis,properties and applications"; *Materials Science and Engineering R* (2006) 52; 49.
- [27] Q Liu, Y Liu, F Wu, X Cao, Z Li, M Alharbi, AN. Abbas, M R. Amer, C Zhou, Highly Sensitive and Wearable In<sub>2</sub>O<sub>3</sub> Nanoribbon Transistor Biosensors with Integrated On-Chip Gate for Glucose Monitoring in Body Fluids, *ACS Nano* (2018), 12, 2, 1170–1178
- [28] M Shariati ,M Sadeghi, Ultrasensitive DNA biosensor for hepatitis B virus detection based on tin-doped WO<sub>3</sub>/In<sub>2</sub>O<sub>3</sub> heterojunction nanowire photoelectrode under laser amplification *Analytical and Bioanalytical Chemistry* (2020) 412, 5367–5377.
- [29] K. Shan, F. Zhai, Z. Yi, X. Yin, D. Dastan, F. Tajabadi, A. Jafari, S. Abbasi, Mixed Conductivity and the Conduction Mechanism of the Orthorhombic CaZrO<sub>3</sub> based Materials, *Surf. Interfaces* (2021) 23 ;100905.
- [30] S. Nie, D. Dastan, J. Li, W. Zhou, S. Wu, Y. Zhou, X. Yin, Gas-sensing selectivity of n-ZnO/p-Co<sub>3</sub>O<sub>4</sub> sensors for homogeneous reducing gas, *J. Phys. Chem. Solids*, (2021) 150 ;109864.
- [31] L. Tao, J. Huang, D. Dastan, T. Wang, J. Li, X. Yin, Q. Wang, New Insight into Absorption Characteristics of CO<sub>2</sub> on the Surface of Calcite, Dolomite, and Magnesite, *Appl. Surf. Sci.*, (2021) 540 ;148320.
- [32] K. Shan, Z. Yi, X. Yin, D. Dastan, S. Dadkhah, B. Coates, H. Garmestani, Mixed conductivities of A-site deficient Y, Cr-doubly doped SrTiO<sub>3</sub> as novel dense diffusion barrier and temperature-independent limiting current oxygen sensors, *Adv. Powder Technol.* 31 (2020) 4657–4664.
- [33] M. Asadzadeh, F. Tajabadi, D. Dastan, P. Sangpour, Z. Shi, N. Taghavinia, Facile deposition of porous fluorine doped tin oxide by Dr. Blade method for capacitive applications, *Ceram. Int.* (2021) 47; 5487–5494.
- [34] L. Tao, J. Huang, D. Dastan, T. Wang, J. Li, X. Yin, Q. Wang, CO<sub>2</sub> capture and separation on charge-modulated calcite, *Appl. Surf. Sci.* (2020) 530 ;147265.

- [35] J. Y. Lao, J. Y. Huang, D. Z. Wang and Z. F. Ren; "Self-assembled In<sub>2</sub>O<sub>3</sub> nanocrystal chains and nanowire networks"; *Adv. Mater* (2004) 16 ;65.
- [36] M Shariati, S Alishavandi, Phototransistor Properties of Indium Tin Oxide Nanowires Grown by RF Sputtering Mechanism and Annealing Process, *Nano* 10 (01), 1550006
- [37] M Shariati, The ITO-Capped WO<sub>3</sub> Nanowires Biosensor Based on Field Effect Transistor in Label-Free Protein Sensing, *Applied Physics A* (2017)123 (5), 370,
- [38] Z. L. Zhan, J. Q. Xu and D. G. Jiang; "State of In<sub>2</sub>O<sub>3</sub>-based gas sensor"; *Chin. J. Trans. Technol* (2003) 22 ;1.
- [39] J. T. Hu, T. W. Odom and C. M. Lieber; " Chemistry and Physics in One-Dimension: Synthesis and Properties of Nanowires and Nanotubes" *Acc.Chem. Res* (1999) 32 ;435.
- [40] M.H. Huang, S. Mao, H. Feick, H. Yan, Y. Wu, H. Kind, E. Weber, R. Russo and P. Yang; " Room-Temperature Ultraviolet Nanowire Nanolasers"; *Science* (2001) 292 ;1897.
- [41] O. Hayden, A.B. Greytak, D.C. Bell; "Core-Shell Nanowire Light-Emitting Diodes"; *Adv. Mater* (2005) 17 ;701.
- [42] X. Y. Kong and Z. L. Wang; "Structures of indium oxide nanobelts"; *Solid state communications* (2003) 128 ;1.
- [43] S. Pareek, U. Jain, M. Bharadwaj, N. Chauhan, A label free nanosensing platform for the detection of cervical cancer through analysis of ultratrace DNA hybridization, *Sensing*, (2021), 33, 100444]
- [44] J. R. Espinosa, M. Galván, A. S. Quiñones, J. L. Ayala, V. Ávila, S. M. Durón, Electrochemical Resistive DNA Biosensor for the Detection of HPV Type 16, *Molecules* (2021), 26(11), 3436.
- [45] B Kang, U Yeo, KH Yoo, Anodized aluminum oxide-based capacitance sensors for the direct detection of DNA hybridization. *Biosensors and Bioelectronics*, (2010) 25; 1592–1596
- [46] YJ Kim, YJ Kim, JE Jones, H Li, H Yampara-Iquise, G Zheng, C A Carson, M Cooperstock, M Sherman, Q Yu, Three-dimensional (3-D) microfluidic-channel-based DNA biosensor for ultra-sensitive electrochemical detection. *Journal of Electroanalytical Chemistry*, (2013) 702; 72–78
- [47] S Wu, WW Ye, M Yang, M Taghipoor, R Meissner, J Brugger, P Renaud, Impedance sensing of DNA immobilization and hybridization by microfabricated polycarbonate nanopore templates. *Sensors and Actuators B*, (2015) 216; 105–112
- [48] A Santos, T Kumeria, D Losic, Nanoporous anodic aluminum oxide for chemical sensing and biosensors. *Trends in Analytical Chemistry*, (2013) 44
- [49] MM Rahman, XB Li, NS Lopa, SJ Ahn, JJ Lee, Electrochemical DNA Hybridization Sensors Based on Conducting Polymers. *Sensors*, (2015) 15; 3801-3829
- [50] W Ye, Y Xu, L Zheng, Y Zhang, M Yang, P Sun, A Nanoporous Polycarbonate Template Based Electrochemical Biosensor for Histamine Determination with Biofunctionalized Magnetic Nanotubes Concentration and Signal Amplification. *Sensors*, (2016) 16; 1767
- [51] A Bonanni, MI Pividori, M del Valle, Impedimetric detection of influenza a (H1N1) DNA sequence using carbon nanotubes platform and Au nanotubes amplification. *Analyst* (2010) 135(7):1765– 1772.
- [52] X. S. Peng, Y. W. Wang, X. F. Wang, L. X. Zhao, G. W. Meng and L. D. Zhang; "Large-Scale synthesis of In<sub>2</sub>O<sub>3</sub> nanowires"; *Appl. Phys. A* (2002) 74 ; 437.
- [53] Y. Tan, X. Wei, M. Zhao, B. Qiu, L. Guo, Z. Lin, H. H. Yang, "Ultra-selective homogeneous electrochemical biosensor for DNA species related to oral cancer based on nicking endonuclease assisted target recycling amplification", *Anal Chem* (2015) 87 ; 9204-9208.
- [54] Yi-Tao Long, Chen-Zhong Li, Todd C. Sutherland, Heinz-Bernhard Kraatz, and Jeremy S. Lee, "Electrochemical Detection of Single-Nucleotide Mismatches: Application of M-DNA ", *Anal. Chem.* (2004) 76 ; 4059-4065
- [55] P. Takmakov, I. Vlassiuk, S. Smirnov, "Hydrothermally shrunk alumina nanopores and their application to DNA sensing", *Analyst* (2006) 131 ; 1248-1253

- [56] Z. G. Gokce, P. Akalin, F. N. Kok, A. S. Sarac, "Impedimetric DNA biosensor based on polyurethane/poly(m-anthranilic acid) nanofibers", *Sens Actuators B* (2018) 254 ; 719–726
- [57] S Jampasa S, W Wonsawat, N Rodthongkum, W Siangproh, P Yanatatsaneejit, T Vilaivan, O Chailapakul; Electrochemical detection of human papillomavirus DNA type 16 using a pyrrolidiny peptide nucleic acid probe immobilized on screen-printed carbon electrodes. *Biosens Bioelectron* (2014) 54:428–434.
- [58] DS Campos-Ferreira, GA Nascimento, EVM Souza, MA Souto-Maior, MS Arruda, DML Zanforlin, MHF Ekert, D Brunaska, JL LimaFilho; Electrochemical DNA biosensor for human papillomavirus 16 detection in real samples. *Anal Chim Acta* (2013) 804:258– 263.
- [59] DS Campos-Ferreira, EVM Souza, GA Nascimento, DML Zanforlin, MS Arruda, MFS Beltrão, AL Melo, D Brunaska, JL LimaFilho; Electrochemical DNA biosensor for the detection of human papillomavirus E6 gene inserted in recombinant plasmid. *Arab J Chem* (2016) 9(3):443–450.
- [60] RE Sabzi, B Sehatnia, MH Pournaghi-Azar, MS Hejazi; Electrochemical detection of human papilloma virus (HPV) target DNA using MB on pencil graphite electrode. *J Iran Chem Soc* (2008) 5(3): 476–483.
- [61] JP Bartolome, L Echegoyen, A Fragoso; Reactive carbon Nano-onion modified glassy carbon surfaces as DNA sensors for human papillomavirus oncogene detection with enhanced sensitivity. *Anal Chem* (2015) 87(13):6744–6751.